Hyper-Physiological Compression Triggers Osteoarthritic features in a Cartilage-on-Chip Model

Paola Occhetta[$a], Andrea Mainardi[$a,b], Emiliano Votta[b], Queralt Vallmajo-Martin[c], Martin Ehrbar[c], Ivan Martin[a], Andrea Barbero*[a], Marco Rasponi[b]

[a] Departments of Surgery and of Biomedicine, University Hospital Basel, University of Basel, Basel, Switzerland

[b] Departments of Electronics, Information and Bioengineering, Politecnico di Milano, Milano, Italy

[c] Department of Obstetrics, University Hospital Zurich, Zurich, Switzerland; Zurich Centre for Integrative Human Physiology, Zurich, Switzerland.

[$] Paola Occhetta and Andrea Mainardi contributed equally to this work.

*Corresponding author: Andrea Barbero, Andrea.Barbero@usb.ch

Abstract (175 words)

Osteoarthritis (OA) is the most common human musculoskeletal disease. Its social impact is expected to increase dramatically due to population ageing but therapy is still limited to palliative treatments or surgical intervention. The shortage in OA disease modifying (DMOA) drugs is mainly related to the absence of valid OA pre-clinical models and the demand for innovative *in vitro* tools able to reliably predict DMOA drug efficacy is therefore urgent. In this study, we developed a microscale platform enabling, for the first time, the application of a finely strain-controlled compression to a 3D microconstruct. Upon generation of an *in vitro* model of human Cartilage-on-Chip (CoC), we demonstrated that a 30% confined compression, recapitulating mechanical factors involved in OA pathogenesis, is sufficient to induce OA traits, accounting for i) a shift of cartilage homeostasis towards catabolism and inflammation, ii) triggering of hypertrophy and, iii) acquisition of a gene profile correlating with clinical OA evidences. As demonstrated by a proof-of-principle pharmacological validation, the presented CoC model represents a powerful tool to potentially screen the potency of DMOA candidates.

Introduction

Osteoarthritis (OA) is the most prevalent human musculoskeletal disease[1]. The incidence of symptomatic OA is expected to increase due to the aging of the population, making OA the worldwide fifth leading cause of disability by 2020[2]. Despite the high prevalence, however, no effective pathology-reversing treatment is currently available and this makes the research for new therapies extremely urgent.

OA is a multifactorial disease characterized by a whole joint pathological active response to environmental factors, being abnormal mechanical loading and oxidative stresses among the most relevant[3]. Such factors trigger an unbalance of anabolic/catabolic activities, which causes a dysfunction of articular chondrocytes and the onset of inflammation, eventually resulting in cartilage degeneration and alterations of subchondral bone, synovium and ligaments[4]. The multifactorial etiology of the disease increases the difficulty in generating relevant pre-clinical models of OA[5]. *In vivo* models provide a better reflection of the naturally-occurring whole-joint disease, but they are costly and time consuming; furthermore, a paradigmatic shift towards the 3R principles in preclinical studies makes *in vitro* modeling of the disease highly desirable[6]. However, currently available *in vitro* models are too simplistic and often fail in predicting drug candidates effects thus calling for more complex and physiological systems[5].

Articular cartilage's extracellular matrix (ECM) is a complex environment whose biochemical composition and hierarchical structure allow a lifelong withstanding of cyclic loading with up to 300% of the body weight[7,8]. Specifically, cartilage ECM is composed by a fluid phase consisting of water and electrolytes, and a solid phase, primarily constituted by fibrillar and non-fibrillar collagens (mainly collagen type-II and type-I, but also type-VI, IX and XI), negatively charged proteoglycans (PGs) (mostly aggrecan and lubricin) and hyaluronic acid[3,8]. Physiological compression of articular cartilage induces a complex mechanical environment that is characterized by stresses, strains, osmotic and hydrostatic pressures, interstitial fluid flow and electrokinetic effects varying in time and space[8–10].
Lately, three-dimensional (3D) macroscale systems integrating cells, soluble factors and ECM-like matrices have been used to model articular cartilage, aiming at recapitulating both cellular specific architecture and mechanical environment[9,11,12]. Whilst holding huge promises as grafts to promote repair of joint injuries[13,14], the generation of such engineered cartilage constructs requires bioreactor systems which may be bulky and hard-to-use bioreactor systems, thus prevent their wide-spreading as *in vitro* models[15].

Difficulties in reproducing *in vitro* a cartilaginous tissue increase when trying to recapitulate a pathological, OA cartilage status. Current *in vitro* models rely either on biochemical (cytokine-based) or mechanical (load-based) stimulation. Cytokine-based models are, however, built on over-dosages of inflammatory cocktails, which induce a downstream effect rather than recapitulating the actual OA environment found *in vivo*[5]. On the other hand, load-based models hold the potentiality of triggering an OA-like response without the need for supraphysiological doses of biochemical stimuli. Indeed, increasing evidence correlates mechanical abnormalities such as obesity, trauma, or joint misalignment to OA onset[3], classifying the biomechanical environment as a key player involved in disease evolution. Load-based models introduced so far are largely based on macroscale bioreactors and were instrumental in defining a background on the mechanism involved in the pathological load response[16,17]. However, they often fail in finely tuning the stimuli provided to the tissue and thus in capturing the native joint physiological/pathological environment[18]. Existing load control systems, on one side, do not account for pathophysiological levels of compression, while strain-controlled devices are affected by reaction forces largely dependent on scaffolds' mechanical responses[5].

Organs-on-chip are an emerging technology able to recapitulate organ functions into microscale platforms, with unprecedented adherence to pathophysiological conditions[6,19]. Recent advances in microfabrication techniques allowed to precisely control the 3D architecture of cellular compartments[20], while integrating medium perfusion, delivery of soluble factors and accurate biophysical stimulation (i.e. 3D mechanical stimuli)[21–23]. These unique characteristics currently make organs-on-chip technology an extremely promising candidate for pre-clinical drug screening. Furthermore, they proved advantages of reduced reagents requirement and ease of manipulation, which makes them particularly appropriate for high-throughput discovery campaigns[24]

In this study, we developed a microscale platform able to reproducibly generate *in vitro* models of human Cartilage-on-Chip (CoC). Thanks to a unique mechanical actuation system, recapitulating the mechanical stimuli involved in OA pathogenesis and specifically compression as main components of cartilage deformation, OA traits can be induced in our CoC both shifting matrix deposition/resorption balance towards catabolism and triggering a gene profile correlated with clinical OA evidences. Clinically approved and novel anti-inflammatory/anti-degrading drugs were administered to the established

osteoarthritic CoC model, proving its potentiality to serve as an effective pre-clinical tool for testing new DMOA candidates in a predictive fashion.

Results

Microscale platform for 3D mechanical confined compression

A microscale platform was conceived to apply a uniform and confined mechanical compression to a 3D cartilage microconstruct (Fig. 1a). The platform comprises two chambers divided by a flexible membrane (Fig. 1b): i) an upper culture chamber hosting the 3D microconstruct, and ii) a lower chamber exploited as actuation compartment. All components were realized in polydimethylsiloxane (PDMS) and assembled as schematically depicted in Fig. SI1. Specifically, the culture chamber consists in a 300µm wide central channel hosting the 3D microconstruct (Fig. 1b, blue channel), surrounded by two side channels for culture medium supplementation (Fig. 1b, red channels). Based on a concept previously developed by our group[23], the central channel is limited by two parallel arrays of hanging posts, conceived with the double function of i) confining a cell-laden pre-polymer solution throughout the seeding and polymerization phases and subsequently ii) defining a stroke length controlling the mechanical actuation mechanism. In rest position (Fig. 1c), a gap divides the hanging posts from the flexible membrane, maintaining the 3D microconstruct in a relaxed state. Upon pressurization of the actuation compartment, the flexible membrane bends upwards till it abuts against the posts' bottom ends (Fig. 1d), causing a confined compression of the 3D microconstruct. When the pressure is released, elastic recoil causes the membrane and the 3D microconstruct to relax to their original rest configurations. Notably, the proposed microscale platform allows to precisely tailor the level of mechanical compression by tuning the gap underneath the hanging posts. In this study, in particular, two gap sizes were designed to achieve a 10% and a 30% compression level, respectively (Fig. SI2). Furthermore, the shape of the posts was specifically conceived to minimize the lateral expansion of the 3D microconstruct during compression, while permitting mass exchanges at the interface between cells and culture medium. In details, a T-shaped resistant section was selected to minimize posts' outward bending arising from the increased pressure generated upon 3D microconstructs compression, and a 30µm gap was chosen to separate consecutive posts from to each other (Fig. 1b, white features). The actuation compartment included two rows of scaffolding posts to prevent from membrane buckling. A picture of the assembled platform

is shown in Fig. 1e, while Fig. 1f extrapolates a detail depicting the T-shaped hanging posts.

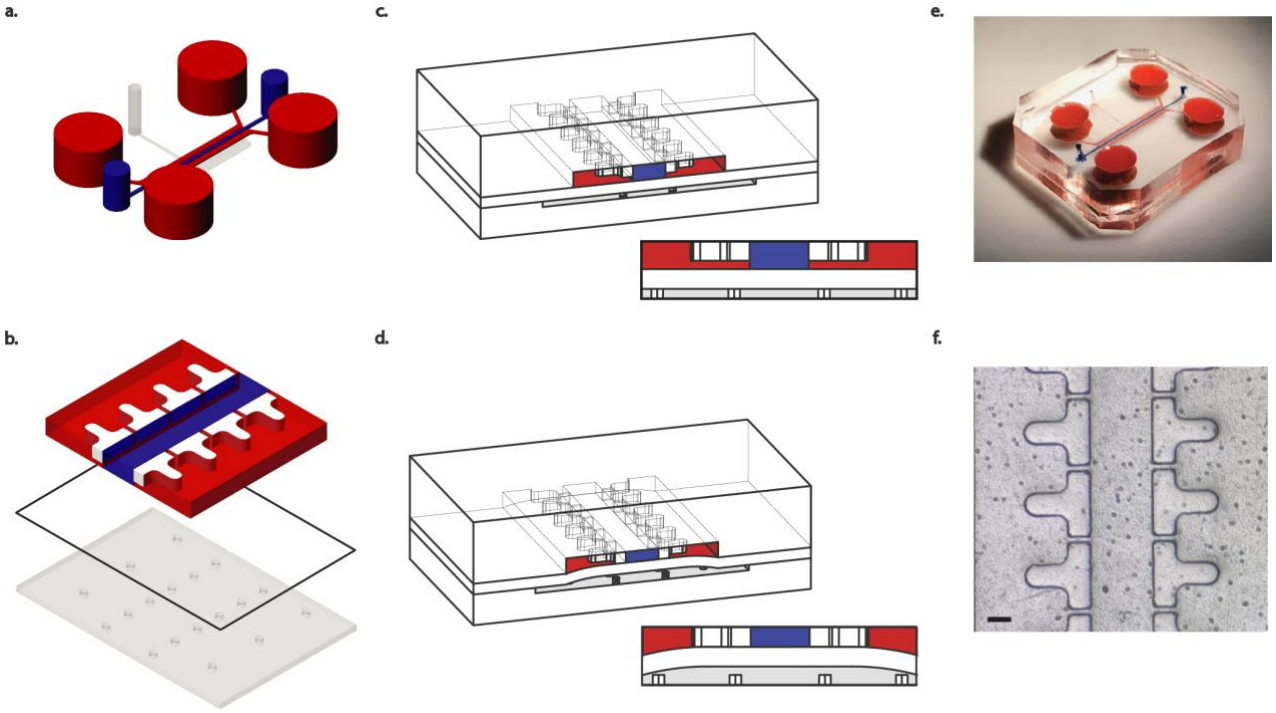

Fig. 1 Microscale platform for mechanical confined compression of 3D cell microconstructs. **a, b,** The microscale platform consists in two compartmentalized PDMS microchambers, featuring configurable geometries and separated by a PDMS membrane. The top compartment is subdivided, by means of two rows of T-shaped hanging posts (white), into a central channel hosting the 3D microconstruct (blue) and two side channels for medium supplementation (red). The bottom chamber (grey) represents the actuation compartment. **c, d,** By pressurizing the bottom compartment, the PDMS membrane deforms, compressing the 3D microconstruct and eventually abutting against the posts' ends, causing a confined compression of the microconstruct. **e,** Picture of an actual assembled platform. **f,** Inset of the T-shaped posts viewed from above. (Scale bar, 100 µm).

Providing confined compression: strain field determination

The gel deformation field associated with the highest compression level (30%) was evaluated through a finite element model (FEM). An enzymatically cross-linked and MMP-degradable poly (ethylene glycol) (PEG) based hydrogel[25] was considered to provide cells with a tissue-mimicking 3D environment. Likewise cartilage, hydrogels exhibit a largely non-linear and strain rate-dependent behaviour resulting from the interaction between the two material constituents, namely a solid matrix and an incompressible permeating fluid, as well as from the inherently viscoelastic property of the former and the viscosity of the latter[26,27]. A biphasic poroelastic (BPE) constitutive model was introduced to model the

cell-laden hydrogel, enabling, while underestimating the reaction forces of the cartilaginous tissues under compression, to accurately predict the corresponding lateral expansion[28]. Model parameters were inferred from literature data on PEG-based hydrogels. In details, Young modulus, Poisson's ratio and permeability of 0.1 MPa[25,26,29], 0.33[30] and 1.72x10-15 m^4/Ns[31], respectively, were considered. Owing to the periodic geometry of the channel, as well as to its symmetry (Fig. SI2), a minimal region of interest, comprising half T-shaped hanging post and the correspondent hexahedral PEG gel region, was adopted in computations (Fig 2a, Fig SI3). Nominal strains (NE_{xx}, NE_{yy}, NE_{zz}) were evaluated to estimate lateral and longitudinal expansion values associated to the hydrogel compression along the z-direction (Fig 2b, Movie S1). A random point-cloud was generated within the control volume: for each point, the closest node of the computational grid was selected; based on the displacement of the selected nodes nominal strains were computed. FEM predictions attested low and overall uniform axial and lateral strain values in the control volume (Median ± SD, of 1.76% ± 0.22% and 0.02% ± 0.006% for NE_{xx} and NE_{yy}, respectively), with peak values in lateral and longitudinal expansion appearing near the windows between posts.

Numerical results were validated experimentally. First, a calibration allowed the definition of the pressure to be applied to the actuation chamber to achieve contact between the flexible membrane and the hanging posts upon stimulation (Fig. SI4). Then, the strain field upon compression was evaluated. The central culture chamber was filled with PEG laden with polystyrene beads (diameter 10 μm). Lateral and longitudinal expansions were assessed measuring beads' displacements upon subjecting the gel to the desired compression (Fig. 2c). Experimental values of 2.21±2.20% and 0.59 ± 2.38% along X and Y, respectively, were in good accordance with numerical estimations (Fig. 2d) and confirmed the achievement of a uniform confined compression state.

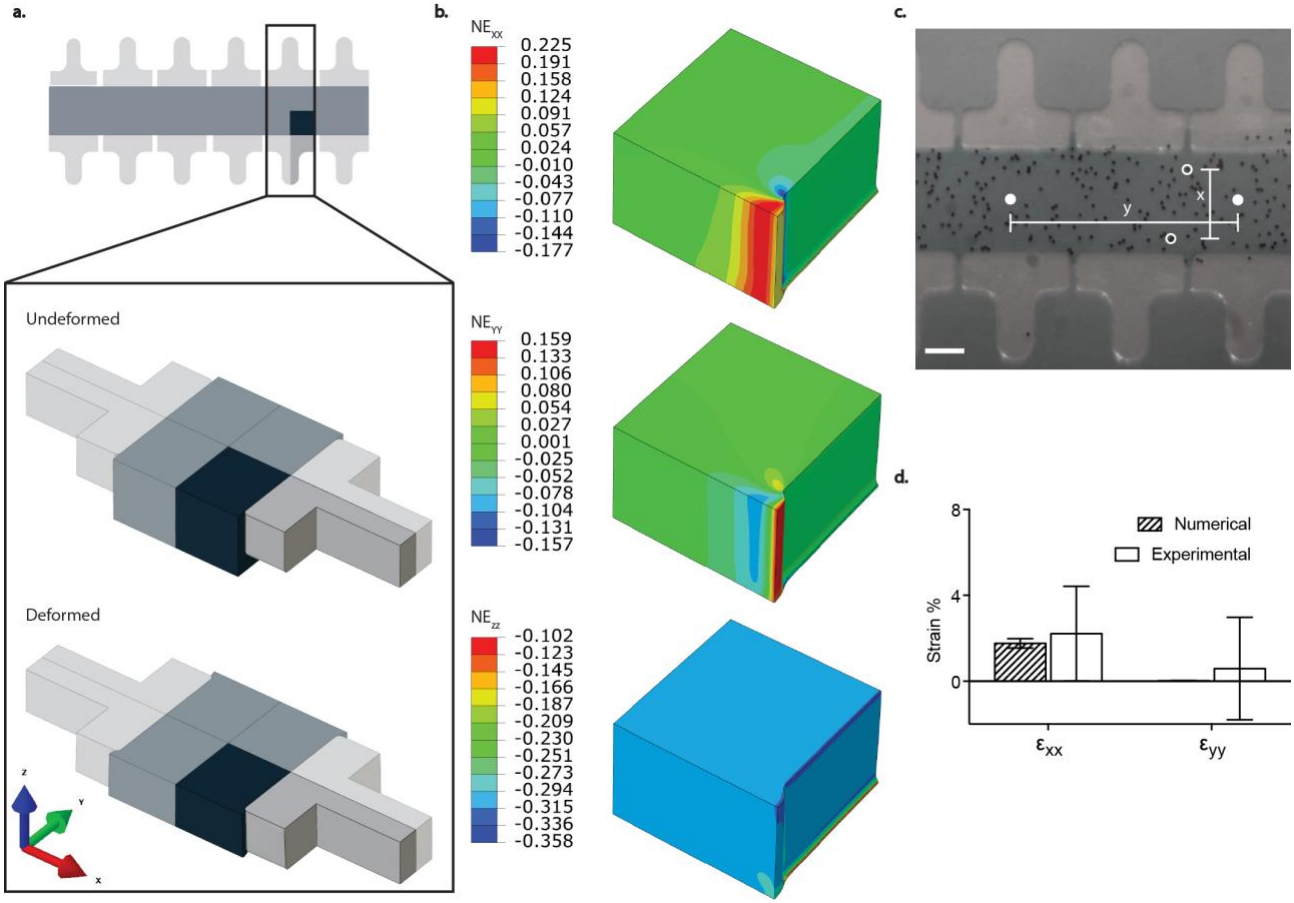

Fig.2 Constructs deformation field: computations and experimental validation. a, Top view and 3D schematization of the region considered in computations. The minimal region of interest is shaded. Symmetry planes were considered as boundary conditions. Both the rest position (Undeformed) and the compressed gel state (Deformed) are displayed. **b,** Strain deformation field normal directions. The strain field is reported through Nominal strains (NE) values in the normal directions XX, YY and ZZ. Lateral and longitudinal expansions are limited in the central gel constructs and the strain distribution is homogeneous. Peaks appear in correspondence of the windows between posts. **c,** Experimental evaluation of the deformation field. Polystyrene beads were embedded in PEG gel. The beads displacement was assessed upon compression of the gel and strains measured along X and Y, resulting respectively equal to 2.21% ± 2.20% and 0.59% ± 2.38%. White dots and clear circles are representative of two couple of beads used for strain measurement along X and Y respectively. (Scale bar, 100 μm; picture showing the deformed state). A total of n=9 independent experiments was considered. 7 couples of beads per experiment were used in assessing the strain along each direction. **d,** Resulting NExx and NEyy predicted numerically and estimated experimentally were compared. Experimental results show good adherence to computational estimates for strains along both the X (ε_{xx}) and Y(ε_{yy}) directions. Data are plotted as mean ±SD. A total of 63 couples of beads (for experimental results) and nodes (for computational results) was considered for each direction.

Establishment of a model of human CoC

The microscale device was first used to establish a model of healthy human Cartilage-on-Chip (CoC). Human articular chondrocytes (hACs) isolated from healthy donors (n=5)

were embedded in PEG gel and injected into the microscale platform (Fig. SI5a, Fig. SI6a). After 14 days of chondrogenic conditioning under static regimen (Fig. SI5b), a cartilage microconstruct was obtained. Notably, the 3D microconstruct was still confined within the two arrays of hanging posts (Fig. SI6b), thus ensuring the geometrical control over the subsequently imposed mechanical stimulation. Immunofluorescence analysis revealed a high deposition of cartilaginous proteins upon two weeks of differentiation. In details, a dense extracellular matrix rich in collagen type-I, collagen type-II and aggrecan was detected at day 14 (Fig. 3a). Collagen type-I and aggrecan were already slightly expressed by hACs at day 0 but remained mostly intracellular up to day 3. Quantification of glycosaminoglycans (GAGs) synthesized during the culture period confirmed a statistically significant increase of GAGs at day 14, as compared to both day 0 and day 3 (Fig. 3b). Gene expression analysis through real-time quantitative PCR (RT-qPCR) also indicated an upward trend in *COL2A1/COL1A1* ratio during the two weeks of differentiation, approaching the level found in native cartilage (Fig. 3c). The time course of articular cartilage signature genes expression was also assessed by RT-qPCR (Fig. 3d). Expression of the articular cartilage-specific genes aggrecan (*ACAN*) and lubricin (*PRG4*), significantly increased during the culture and matched at day 14 the level of the genes detected in native chondrocytes. Specifically, *ACAN* expression showed a constant increasing trend along the two differentiation weeks, while PRG4 expression was already highly upregulated after three days. The expression of *GDF5* and autotaxin *(ATX)*, low in native adult chondrocytes and associated with joint interzone embryonic development[32] and regulation of cartilage formation[33], increased over time, with the expression of *ATX* reaching a plateau already after three days. Finally, expressions of wingless-type MMTV integration site (Wnt) antagonist Frizzled-related protein (*FRZb*) and Bone Morphogenetic Protein (BMP) antagonist Gremlin-1 (*GREM1*), genes expressed in adult hACs[34], were characterized by a statistically significant upward trend during the two weeks of culture, again approaching after 14 days the level found in native chondrocytes.

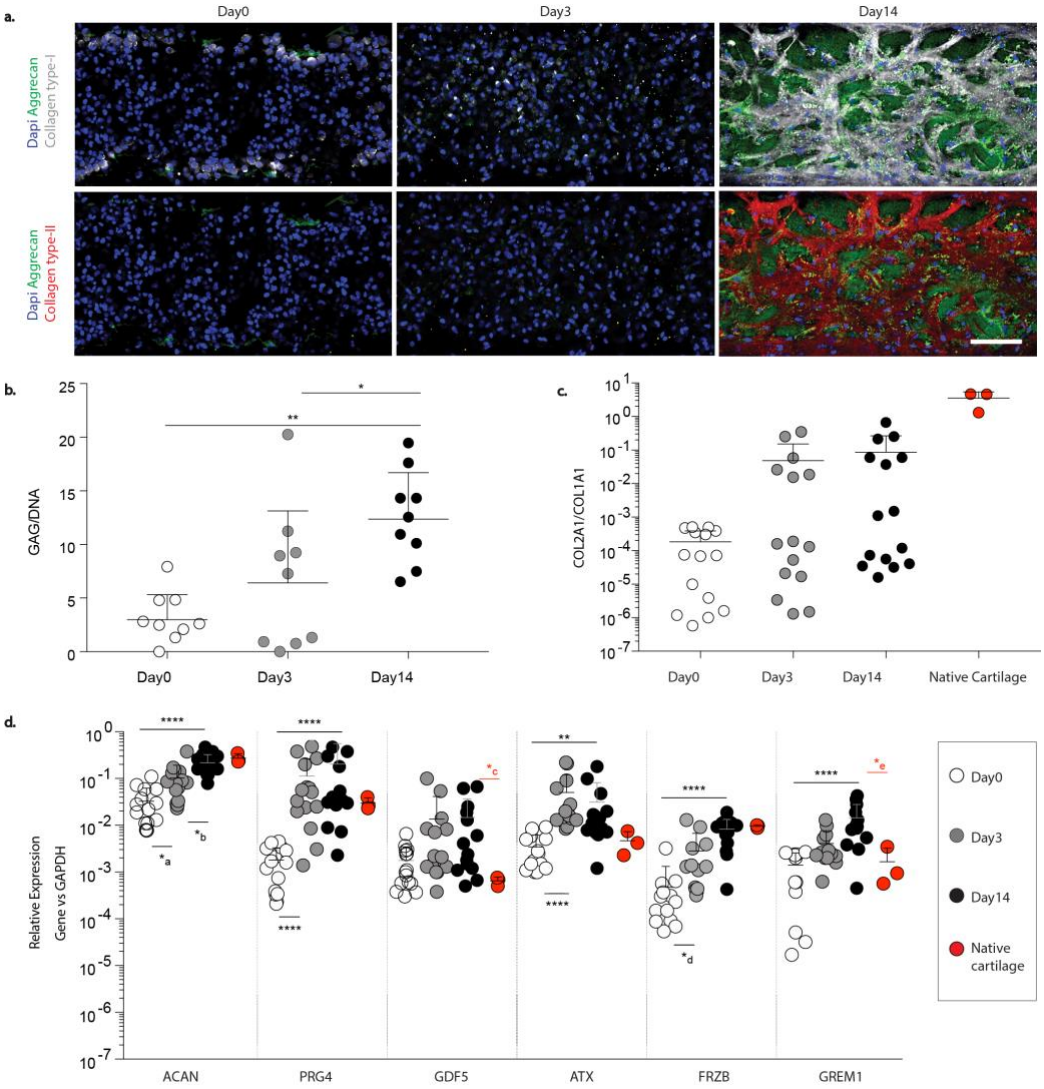

Fig. 3 Establishment of a human model of healthy CoC. a, Aggrecan, collagen type-I and collagen type-II expression was assessed by immunofluorescence, revealing a dense cartilage-like extracellular matrix deposition upon 14 days of differentiation (representative pictures. Scale bar, 100 µm). **b,** CoC maturation was also confirmed by the statistically significant increase in GAG production during the 14 days of differentiation. Statistics by One-way ANOVA with Bonferroni's, single pooled variance, multiple comparison test. *P = 0.0446, **P= 0.0011. n=9 biologically independent samples from 3 different donors were considered **c,** the *COL2A1/COL1A1* expression ratio (n=15 biologically independent samples from 5 different donors) and **d,** the time course expression of a panel of genes characterizing articular cartilage were quantified by RT-qPCR and compared with expression level in native healthy chondrocytes (in red, n=3 biologically independent samples from 5 different donors). All gene expression values are normalized relative to GAPDH expression and values are log scale. n=15 biologically independent samples from hAC of 5 different donors were generated and analysed; results are expressed as mean (centre values) + SD (measure of dispersion), *a P = 0.0268, *b P = 0.0237, *c P = 0.0353, *d P = 0.019, *dP = 0.0393, **P = 0.0021, ***P < 0.001 ****P<0.0001). Statistics by one way ANOVA and Bonferroni's multiple comparison tests (normal distributions), or Kruskal-Wallis test with Dunn's multiple comparison test (non-normal distributions) in all graphs where statistical analysis is reported. A two tailed Mann-Whitney test was used to compare gene expression of cells cultured in the device for 14 days and of a pool of 5 healthy donors. Statistical significance is indicated in red.

Effect of mechanical compression on CoC anabolism

The microscale device was then used to mechanically control the environment of the achieved CoC. Mechanical stimulation was applied through an electro-pneumatical actuation system (Fig. SI7). Upon 14 days of maturation, the established CoC model underwent seven days of mechanical stimulation at different levels of compression. Specifically, either Physiological (10%, PC) or Hyper-Physiological (30%, HPC) Compression was delivered, with a pattern resembling the daily walk routine (i.e. frequency 1Hz, 2h stimulation, 4h rest, 2h stimulation, 16h rest per day) (Fig. SI5c). Control devices were cultured under static conditions during the stimulation period. HPC was tested for direct cell death through LIVE/DEAD assay and negligible cellular death was detected (Fig. SI8). GAG production was not affected by any compression regimen (Fig. 4a) but maintained an increasing trend when compared to the beginning of mechanical stimulation (Fig.3b). HPC however led to a decreasing trend in *COL2A1/COL1A1* mRNA and a significant reduction in *ACAN* mRNA expression, as compared to both control and PC (Fig. 4b, c). This result indicates that the hyperphysiological load condition simulated in the CoC triggers a loss of expression of anabolic genes.

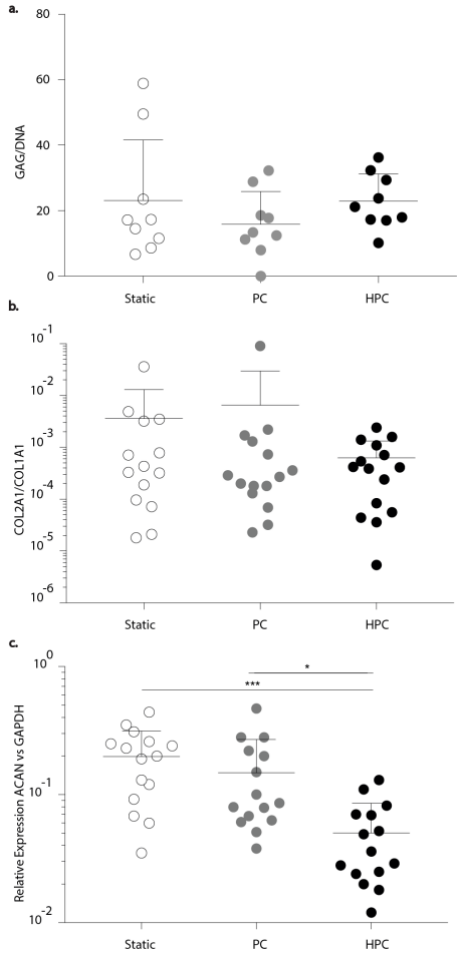

Fig. 4 Effect of mechanical compression on CoC anabolic traits. a, At the protein level, GAG production was not modulated upon mechanical compression. (n=9 biologically independent samples from 3 different donors; results are mean + SD). **b, c,** RT-qPCR analysis revealed a decreasing trend for *COL2A1/COL1A1* mRNA expression upon HPC and a statistically significant down-regulation of *ACAN* mRNA expression in the same condition, as compared to static control and PC. (n=15 biologically independent samples from 5 different, results are mean + SD, *P = 0.0108 ***P < 0.001). All gene expression values are normalized relative to GAPDH expression and values are log scale. Statistics by Kruskal-Wallis test with Dunn's multiple comparison test (non-normal distributions) in all graphs where statistical analysis is reported.

HPC induces MMP-13 production and inflammation

After two weeks of maturation, the effect of seven days of mechanical compression on the CoC catabolic and inflammatory profile was investigated. MMP-13 is the main enzyme responsible for collagen type-II and aggrecan degradation, playing a role in cartilage degeneration[35]. Immunofluorescence analysis revealed that both mechanical compression levels promoted the intracellular expression of MMP-13 (Fig. 5a). However, HPC led to a higher co-localization of DIPEN, an aggrecan MMP-generated C-terminal aggrecan neoepitope[36], within MMP-13 positive cells, suggesting a higher matrix-degrading activity (Fig. 5a, Movie S2). Coherently, HPC induced a statistically significantly higher secretion of pro-MMP13 (Fig. 5b) and enhanced *MMP13* gene expression (Fig. 5c), as compared to both control and PC. Treatment of the CoC with a supraphysiological dose of IL1β (Fig. SI9a, IL1β high) resulted in a similar increase of *MMP13* as compared to static control, while low doses of IL1β didn't affect *MMP13* expression (Fig. SI9a, IL1β low). The degrading effect of mechanical HPC was specific for MMP-13, being *ADAMTS5* expression not modulated among the different conditions (data not shown). The effect of HPC on inflammatory genes expression was also assessed. Interestingly, HPC induced a significant upregulation of a key pro-inflammatory cytokine, namely *IL8*, as compared to both control and PC (Fig. 5c), thus suggesting the onset of inflammation in the model. Moreover, *IL6* expression exhibited a slight increase upon HPC. Again, treatment of the CoC with a supraphysiological dose of IL1β (Fig. SI9b, c IL1β high) resulted in a significant increase of *IL6* and *IL8* as compared to static control, while low doses of IL1β didn't affect their expressions (Fig. SI9a, IL1β low).

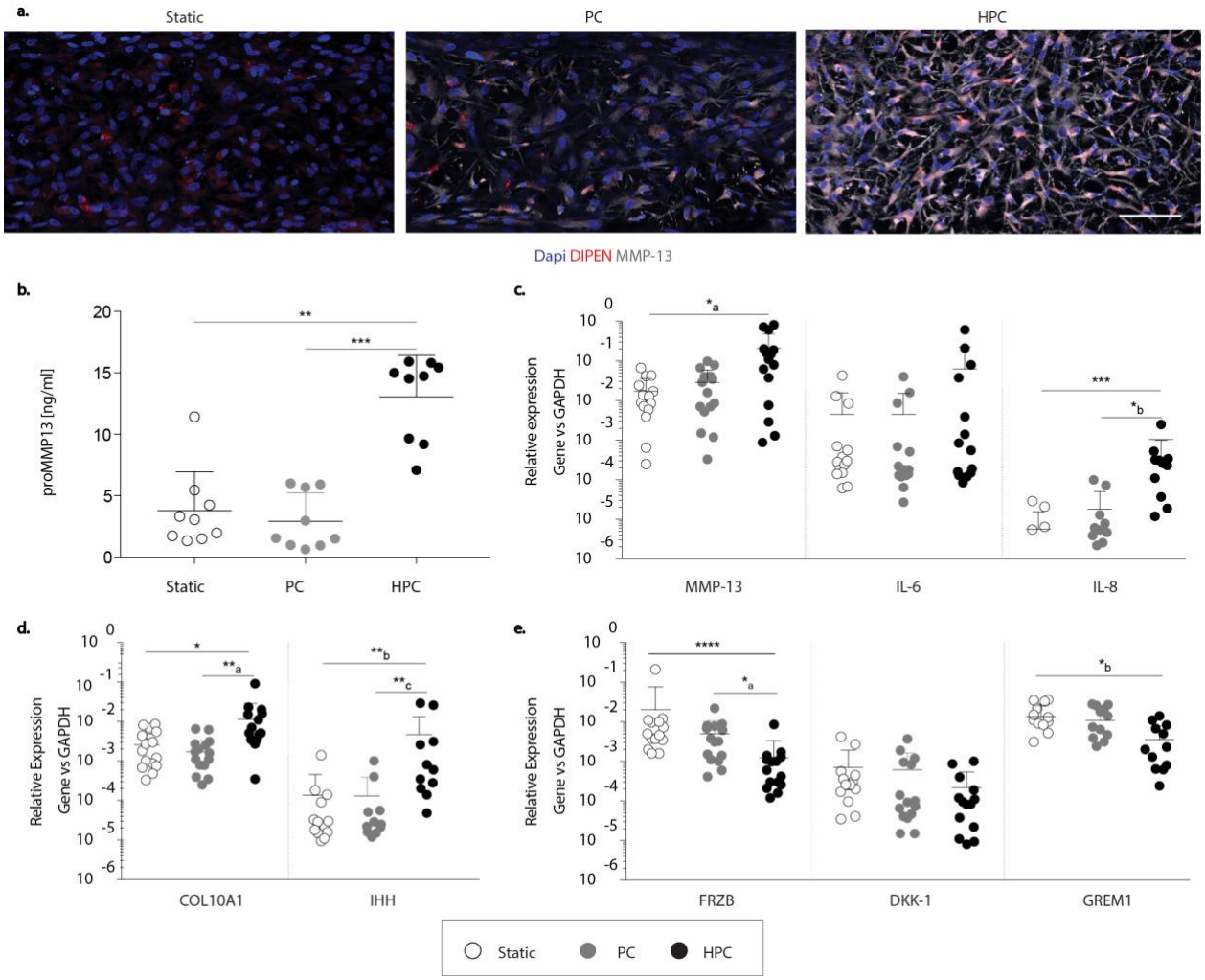

Fig. 5 Effect of mechanical compression on CoC catabolic enzymes, inflammation, hACs phenotypic switch and OA-correlating gene profile. a, MMP-13 (grey) and DIPEN (red) expression were analysed by immunofluorescence staining, revealing a higher intracellular expression of MMP-13 in both mechanical compression conditions. Dapi was used as nuclear counterstaining. (Scale bar, 100 µm). **b,** Pro-MMP13 secreted in the culture medium was quantified and indicated a statistically significant higher production upon HPC, as compared to control and PC. (n=9 biologically independent samples from 3 different donors, statistics by Kruskal-Wallis test with Dunn's multiple comparison test (non-normal distributions) **P = 0.0045, ***P < 0.001). **c,** Expression of genes responsible for matrix degradation and inflammation (*MMP13, IL6, IL8*) was measured by RT-qPCR, indicating unbalance towards a catabolic-preferential and inflamed microenvironment upon HPC. (statistics by Kruskal-Wallis test with Dunn's multiple comparison test (non-normal distributions), n=15 biologically independent samples from 5 different donors; *aP = 0.0307, *b = 0.0337, ***P < 0.001). All gene expression values are normalized relative to GAPDH expression and values are log scale. **d,** Gene responsible for cartilage hypertrophic differentiation (*COL10A1, IHH*) significantly increased their expression upon HPC. (statistics by Kruskal-Wallis test with Dunn's multiple comparison test (non-normal distributions), n=15 biologically independent samples from 5 different donors; *P = 0.0233, **aP = 0.0017, **bP = 0.0018, **cP = 0.0048). All gene expression values are normalized relative to GAPDH expression and values are log scale. **e,** Expression of genes inversely correlated to OA in clinics was down-regulated in the proposed CoC model upon HPC. (statistics by Kruskal-Wallis test with Dunn's multiple comparison test (for non-normal distributions, FRZB and DKK-1),or by one way ANOVA with Bonferroni's multiple comparison tests (normal distributions, GREM1) in all graphs where statistical analysis is reported; n=15 biologically independent samples from 5 different donors; *aP = 0.0109 , *bP = 0.0261 ****P<0.0001). Results are mean + SD.

HPC induces a gene profile correlating with OA

We further characterized the effect of mechanical compression on inducing hypertrophic traits in the CoC. As expected, *COL10A1*, naturally not expressed by healthy hACs, was poorly expressed at a gene level by CoC cultured under static condition. While *COL10A1* expression was not altered upon seven days of PC, HPC induced a significant upregulation of *COL10A1* expression, suggesting the triggering of a hypertrophic differentiation of hACs towards transient chondrocytes (Fig. 5d). Similarly, the expression of Indian Hedgehog (*IHH*), a master regulator of hypertrophic chondrocytes differentiation[37], was significantly increased upon HPC (Fig. 5d). Conversely, the application of IL1β (either at low[38] or high doses[39]) to articular chondrocytes cultured either in monolayer or in 3D within the established CoC model didn't lead to an increase of these genes, thus not mirroring hypertrophic traits characterizing OA progression (Fig. SI10a, b).

BMP and Wnt signalling antagonists *GREM1, FRZB* and dickkopf 1 homolog (*DKK1*) were defined as articular cartilage's natural brakes of hypertrophic differentiation[34] and their expression was inversely correlated with OA onset[40]. Interestingly, the pure application of HPC was sufficient to trigger a significant down-regulation of those genes in our CoC model, with levels matching those detected in native OA hACs (Table S1), thus suggesting the onset of a gene expression profile correlating with OA (Fig. 5e). Treatment of the CoC with a supraphysiological dose of IL1β resulted in a significant decrease of FRZB (Fig. SI9d, IL1β high), while it didn't affect GREM1 or DKK1 expression levels (Fig. SI9e, f, IL1β high). None of these genes were instead modulated by treating the CoC with a low dose of IL1β (Fig SI9, d-f, IL1β low).

Pharmacological validation of the OA CoC model

Upon two weeks of maturation and one week of HPC, a CoC model exhibiting OA-like traits was achieved. This model was thus used to test the effect of drugs, which were already demonstrated to be associated with anti-inflammatory and anti-catabolic effects in preclinical and clinical studies (Fig. SI5d). Notably, serum and TGFβ were removed from the culture medium prior to drug administration, as possible masking/confounding factors. A "cytokine-based" model based on inflammation with a traditionally used high dose of IL1β[39] directly applied within the established CoC model was also included for a preliminary screening over the effect of two selected drugs (i.e. Interleukin-1 Receptor

antagonist (IL1Ra)[41] and Rapamycin). The effects of a broader spectrum of drugs on the expression of *MMP13* (Fig. 6a, Fig. SI11a) and *IL8* (Fig. 6b, Fig. SI11b) were then investigated in the OA-induced CoC, using DMSO as vehicle control (DMSO, 1:5000). Dexamethasone (10μM), a corticosteroid drug that prevents collagen degradation through the inhibition of inflammatory cytokines[42], was used as reference compound[43] and as expected strongly inhibited *MMP13* expression, while not affecting the expression of *IL8*. Both tested doses of IL1Ra[41] induced a statistically significant reduction in the expression of *MMP13* and *IL8* in our CoC model, and a similar trend was detected for *IL8* in the IL1β treated system for the high IL1Ra dose (Fig. SI11a, b). Rapamycin was selected as mTOR activity inhibitor[44], a macrolide compound critical mediator of mechanotransduction involved in the process of cartilage degeneration associated with post-traumatic OA[45]. In the CoC model, Rapamycin reduced the expression of *MMP13* at both tested doses but had a significant effect on *IL8* only at the highest dose (previously shown to increase autophagy[46]). Neither *MMP13* nor *IL8* expression was instead modulated by the same dose of Rapamycin in the IL1β treated system (Fig. SI11a, b). Celecoxib, a non-steroidal anti-inflammatory drug[47], significantly reduced both MMP13 and *IL8* expression in the CoC model.

Once the model was validated on well-established anti-inflammatory/anti-catabolic compounds, a candidate currently under development by Fidia Farmaceutici SpA with proven MMP inhibition activity was tested[48]. The hyaluronic acid alkylamide HYADD®4, contained in the already approved viscosupplement Hymovis® (Fidia Farmaceutici SpA, Italy) and known to exert a competitive inhibition on matrix metalloproteases (MMPs)[49], was supplemented to the system after thermal depolymerization, in order to reduce its viscosity, and compared to unmodified HA of similar low molecular weight (~50 kDa, LMW-HA). The anti-inflammatory effect of the two compounds was comparable in terms of reduction of inflammation, as demonstrated by the decrease in IL8 expression, a pro-inflammatory cytokine that has a key role in the pathophysiology of OA[50] (Fig. 6c). HYADD®4 instead exhibited a statistically significant and selective effect on reducing the expression of MMP13 (Fig. 6d), one of its main hypothesized targets[48], consistent with previous preclinical and clinical reports[51].

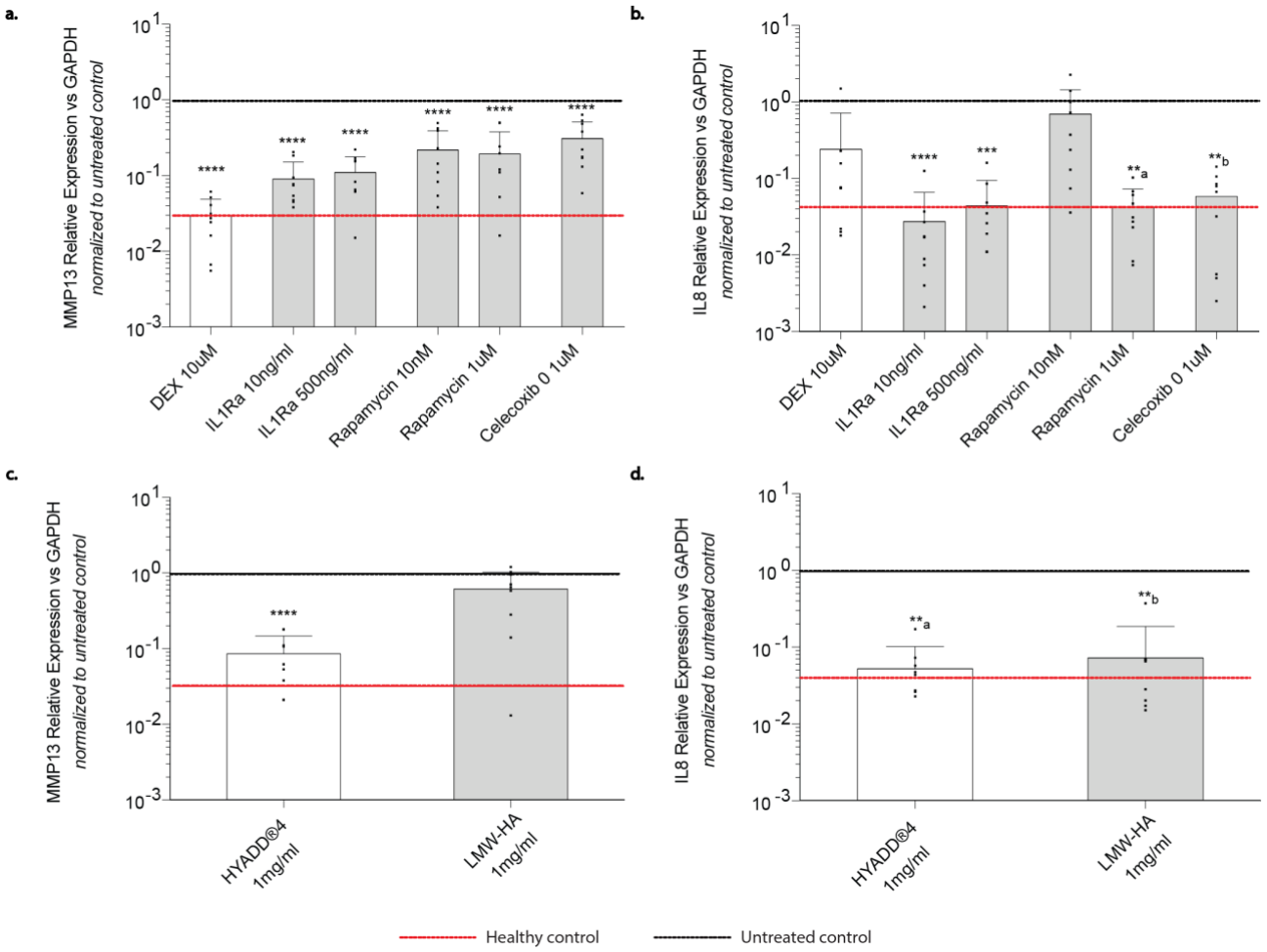

Fig. 6 Drug screening on OA CoC model. a, b, The expression of *MMP13* and *IL8* in response to administration of known anti-inflammatory/anti-catabolic compounds was evaluated by RT-qPCR. Upon generation of the OA CoC model, drugs were supplemented to the culture medium for three days, while maintaining HPC. DMSO was used as vehicle. The mean expression value of the healthy control (i.e. Static CoC) is represented by the red horizontal line, while the mean expression of the untreated control (i.e. HPC CoC supplemented with DMSO only) is represented by the black horizontal line. All gene expression values are normalized relative to GAPDH expression and refer to the basal expression in the untreated control; values are log scale. Statistical significance was calculated against the respective untreated control. (n=9 biologically independent samples from 3 different donors, statistics by one way ANOVA with Dunnett's multiple comparison tests (normal distributions, MMP13) or Kruskal-Wallis test with Dunn's multiple comparison test (non-normal distributions, IL8) **aP = 0.0012, **bP = 0.0030, ***P < 0.001 ****P < 0.0001).**c, d,** The expression of *MMP13* and *IL8* in response to the administration of thermally depolimerized HYADD®4 and low molecular weight HA (~50 kDa, LMW-HA) was evaluated by RT-qPCR. Upon generation of the OA CoC model, drugs were supplemented to the culture medium for three days, while maintaining HPC. DMSO was used as vehicle. The mean expression value of the healthy" control (i.e. Static CoC) is represented by the red horizontal line. All gene expression values are normalized relative to GAPDH expression and refer to the basal expression in the untreated control; values are log scale. (n=9 biologically independent samples from 3 different donors; Statistical significance was calculated against the respective untreated control. Statistics by Kruskal-Wallis test with Dunn's multiple comparison test (non-normal distributions) in all graphs where statistical analysis is reported. **aP = 0.0023, **bP = 0.0016, ****P<0.0001. Results are mean + SD.

Discussion

In the present study, we propose a microscale platform integrating i) a PEG hydrogel-based 3D microenvironment and ii) a mechanical actuation system able to provide defined levels of confined compression, as a tool to generate an *in vitro* model of Cartilage-on-Chip (CoC). The platform was successfully used to elicit the acquisition of osteoarthritic traits by the newly formed cartilaginous tissue, through the sole imposition of a hyper-physiological mechanical stimulation. A proof of principle of the advantageous applicability of the generated OA CoC model as drug screening platform was finally provided.

In the native cartilage, chondrocytes are subjected to a variety of mechanical stimuli, which are yet difficult to recapitulate *in vitro*[10]. Dissecting the complexity of such joint mechanical microenvironment, we here focused on the compressive component, which is representative of the deformation field experienced by chondrocytes[3]. Recent advances in microfluidic and microfabrication technologies have enabled the integration of key mechanical cues (i.e. cyclic uniaxial strain) within 3D *in vitro* models, featuring a cellular relevant scale and an unprecedented level of control[23]. Building upon these cutting-edge technologies, we designed a platform able to apply, for the first time at the microscale, a controlled and confined axial compressive strain to a 3D cell-laden microconstruct, while limiting lateral and longitudinal expansion. Finite element modelling was used to optimize the geometrical features of the device and to evaluate the strain field within the 3D microconstruct volume. Remarkably, an overall homogeneity could be achieved in the Nominal Strains. Homogeneity in the applied mechanical cues indeed avoids exacerbating the response heterogeneity that is inherent to cell populations, thus limiting the presence of uncontrolled and confounding factors. Furthermore, the experimental validation proved a strong correspondence to the *in-silico* computations in terms of confined compression applied over the entire volume of the 3D microconstruct. Existing macroscale bioreactors-based compressive models are either force-controlled or strain controlled. Force-controlled systems often induce not physiologically relevant strains[5], since the associated forces are largely dependent on the mechanical properties of the artificial scaffold[16,17]. Strain-controlled systems, on the other hand, exhibit poor control over the actual provided mechanical stimuli. Compression of biphasic materials such as hydrogels, in fact, induces deformation of the solid component resulting into transient increases in the pressure of the permeating fluid. Pressure equilibrates as the fluid is forced out of the gel, generating unwanted pressure waves. Thanks to the increased surface to volume ratio characterizing

microfluidic systems, a rapid attenuation of the generated waves is instead possible at the microscale, thus avoiding this undesired effect of the matrix-fluid coupling[52]. The proposed device allows to provide a strain-controlled and locally well-defined mechanical stimuli to confined constructs characterised by a cartilage-like ECM, achieving compressive levels tailored to be consistent with those measured *in vivo*[53,54].

The designed microscale platform was first exploited to generate an *in vitro* model of human articular CoC, and subsequently to shift its mechanical microenvironment towards a hyper-physiological level. To this aim, we took advantage of a previously introduced 3D enzymatically cross-linked and MMP-degradable PEG hydrogel matrix[25]. The constitutive PEG hydrogel network is synthetic thus benefitting from a higher standardization with respect to naturally derived biomaterials[55]. Furthermore, it was chemically modified to enable metalloproteinase-mediated degradation, thus permitting tissue remodelling through physiologically relevant processes. By encapsulating adult hACs within PEG hydrogel and culturing them for 14 days, microtissues rich in collagen type-II and aggrecan, constitutive element of the articular cartilage ECM, were obtained. A panel of genes highly expressed in human articular cartilage (i.e. ACAN, PRG4, COL2A1/COL1A1 ratio) were upregulated in the CoC and showed after 14 days of maturation an expression level comparable to that found in native healthy chondrocytes, confirming the physiological relevance of the system as cartilage model. Canonical Wnt inhibitor Frizzled-Related Protein (FRZB) and BMP antagonist Gremlin (GREM1) were recently identified as cartilage brakes of hypertrophic differentiation in adult human cartilage[38]. Their upregulation up to level comparable with native chondrocytes further demonstrates the maturation of the obtained CoC towards a stable articular cartilaginous tissue. Finally, increased expression of ATX and GDF5 over time could indicate an evolution of our model towards stable cartilage through the recapitulation of a developmental pathway[32]. It is worth noting that in our model cells mostly presented an elongated morphology after two weeks of maturation, while an ideal cartilaginous model would comprise chondrocytes with a more round morphology. Nevertheless, the fact that a dense matrix rich in cartilage ECM components could be achieved together with a gene expression panel not dissimilar to that of native chondrocytes make our model adequate in representing the functional response of cartilage on chip. Notably, the presented platform allowed achieving CoC models in a highly reproducible fashion starting from five different human donors, without any exclusion. This demonstrates the capability of the model in generating articular

cartilage constructs, regardless of the reported high donor-to-donor variability proper of primary hACs[56].

A series of clinical evaluations indicates mechanical abnormalities (e.g., due to obesity, trauma, joint misalignment) as one of the key risk factors in developing OA[3]. We thus hypothesized that a hyper-physiological mechanical stimulation could trigger the onset of early OA traits also *in vitro*. Intensity of the strain field in the cartilage upon mechanical compression is currently under debate and its reported values vary depending on the considered region within the joint, on the physical activity undertaken by the subjects and on disease progression[3]. Based on existing reports, two compression levels were chosen as representative of physiological (10%, PC) and hyper-physiological (30%, HPC) mechanical stimulations. While load-based *in vitro* models currently used to induce OA often rely on mechanical stimuli that disregard the *in vivo* joint condition and induce direct cell damage[3,5], the compressive values applied here were demonstrated to modulate inflammation[57], while still falling within the range of cartilage deformations occurring *in vivo*[53,54]. Moreover, cellular viability assays permitted to exclude that the anabolic-catabolic imbalance observed in our model was caused by overload-mediated cellular death[3].

The pathological changes observed in OA joints include a substantial alteration of stable articular cartilage homeostasis, mainly resulting in i) loss of cartilage matrix components, ii) increased inflammation and production of degrading mediators and iii) acquisition of hypertrophic traits. Accordingly, HPC applied in this study was sufficient alone to induce a catabolic imbalance in the CoC model, characterized by reduction of cartilage ECM constituents (i.e. *COL2A1*, *ACAN*), in line with previous findings[58], and by the onset of an inflammatory microenvironment through *IL6* and *IL8* upregulation. Moreover, the production of degrading enzymes (i.e. MMP13) was significantly enhanced in response to HPC, suggesting the triggering of a tissue degradation process. ProMMP13 levels released in the supernatant were incremented only by the HPC, thus suggesting the presence of a triggering threshold for the mechanical overload. The onset of a hypertrophic cartilage phenotype [59] was also observed in our model, with increased gene expression level of *COL10A1* and *IHH* upon HPC. Notably, this trend was not visible when "cytokine-based" model was used, regardless the concentration of IL1β or the dimensional scale of the model (2D vs. 3D), suggesting the better adequacy of our HPC-based system in modelling hypertrophic traits characterizing OA progression.

FRZb, DKK1, inhibitors of Wnt pathway, and *GREM1,* antagonists of BMP pathway, have been reported to play a key role in cartilage homeostasis[60]. A downregulation of these genes was demonstrated in human OA as compared to healthy cartilage, with a further drop in load bearing degraded zones within the same joint[34]. HPC led to a significant reduction of these genes' expression, demonstrating the capability of the presented model to capture the Wnt and BMP antagonists dysregulation reported in osteoarthritis patients. Notably, previous *in vitro* studies[34,60] achieved the downregulation of these genes following cytokine subministration (i.e. IL1β), and their upregulation upon mechanical stimulation within a physiological range. Here, we induced for the first time *in vitro* a downregulation in the expression of these genes upon application of an OA-like hyper-physiological compression.

Presented data demonstrate the capability of the proposed platform to effectively induce cellular responses of our CoC model that have been correlated with the onset of OA in human joints, by the sole imposition of a mechanical hyper-physiological compression. Notably, these responses showed to be strictly dependent on both the compression level and the compression nature (confined) achieved by the specific design (Fig SI12), highly suggesting that they are mediated by mechanobiology rather than mere mass transfer phenomena. It is however worth mentioning that the identification of univocal and commonly accepted biomarkers for determining the switch between healthy and pathological cartilage is still a critical issue in the field. On one hand, the translation of clinically used prognostic and diagnostic biomarkers to *in vitro* systems is still poorly defined; on the other hand, a clear definition of pathways deregulation involved in OA aetiology is still lacking even in the clinical scenario [61]. This huge gap makes the *in vitro* representation of the disease particularly cumbersome and recommends caution in claiming effective mirroring by proposed models of the joint pathology. Overall, a deeper understanding of the pathology basic mechanisms will be pivotal in bridging this gap and eventually defining the ideal *in vitro* model of OA. It is also worth mentioning that OA is a whole joint disease involving cartilage but also osteochondral bone and synovial tissue. While dissecting factors affecting single tissues, as proposed in this study, is instrumental in reducing complexity, the inclusion of multi-tissue interfaces and inter cellular cross-talks[62,63] will be the next essential step towards a "joint-on-chip" perspective.

Even if far from recapitulating a “whole OA joint”, the proposed HPC-based CoC model presents key cellular responses correlated with the onset of OA in the cartilage compartment (i.e. inflammation, catabolism/anabolism unbalance, onset of an hypertrophic phenotype) and it is thus a promising tool for testing the anti-OA effects of drug candidates. We here demonstrated that anti-inflammatory and anti-catabolic responses of both known drugs[41,44,47] and compounds currently under investigation[48] could be predicted by our model. Our results were consistent with data from previously reported animal studies[41,47,64,65], and in some cases were able to predict effects not detectable by a traditional “cytokine-based” model (i.e. effects of Rapamycin).

Outlook

We presented an *in vitro* microscale platform enabling for the first time the application of a finely strain-controlled compression to a 3D microconstruct. We demonstrated the possibility to obtain stable and highly reproducible CoC and to elicit a biological response to mechanical overload, which correlates with key traits triggered during OA onset. Moreover, this model predicted effects of anti-inflammatory/anti-catabolic drugs and results were consistent with existing preclinical and clinical reports. The prediction of drug responses was instead poor in the commonly used cytokine-based model. The proposed platform gives, therefore, a first proof of concept on the possibility of creating miniaturized *in vitro* models closely representing a joint degenerative pathology such as OA. The here presented CoC model will serve both in performing basic research towards a better understanding of OA pathophysiology and, through the implementation of a higher-throughput version[24], as a powerful tool to screen anti-OA candidates, speeding up the discovery process and potentially decreasing the need for animal models.

In a broader perspective, this unique technology could also be beneficial to studying the response to mechanical stimulation of different tissues naturally subjected to deformation under physiological or pathological conditions (e.g., bone), while combining the efficacy of scale reduction with the capability of reproducing key structural and functional cues with unprecedented precision.

Methods

Device design and fabrication

The microscale platform was composed by two layers of polydimethylsiloxane (PDMS, Sylgard 184, Dow Corning) polymerized in defined casts at 10:1 weight ratio of base to curing agent at 65 ºC for at least 3 hours, and a PDMS unpatterned membrane. Master molds were fabricated in a clean room environment using standard photolithography techniques with SU-8 2050 photoresist (MicroChem) on 4" silicon wafers substrates. The cross-sectional size of the features was 1.4 mm (width) x 143 µm (height) for the top layer, and 1.6 mm (width) x 50 µm (height) for the bottom layer. In addition, top and bottom layers included two rows of posts delimiting the culture channel.

Posts in the top layer were fabricated with a T-shaped cross-section; each branch of the T-shape was 300 µm long and 100 µm thick (Fig. 1f). The end of the branch pointing outwards from the culture channel was rounded to avoid air entrapment during device operation. Within each row, posts were separated by a 30 µm gap, and the distance the two rows was 300 µm. Separate molds were fabricated for the physiological and hyper-physiological top layers of the microscale device, i.e., to induce a -10% and -30% vertical compression on the construct. This criterion led to defining gaps by 14 µm and 43 µm, respectively, underneath the posts (Fig. SI2).

Posts in the bottom layer were fabricated with a circular cross-section (radius 30µm), with a 200 µm gap between adjacent posts in the same row, and a 500 µm distance between the two rows.

The membrane separating top and bottom layers was fabricated with a thickness of 750 µm by accurately dosing the PDMS poured on a flat substrate. This value ensured that the membrane's bending stiffness was the sole determinant of the actuation pressure (defined as the pressure required for the membrane to abut against posts bottom ends), independently from the CoC mechanical properties (Fig. SI4). This prevented from undesired changes in the compression stroke throughout the culture period.

The PDMS stamps were peeled off the molds and assembled layer-by-layer as depicted in Figure SI1. Before assembling, the top layer was finalized by punching circular access ports with biopsy punchers: cell in/out ports had a 750 µm diameter, ports for cell culture medium reservoirs had a 5 mm diameter (Fig. SI1). Subsequently, the surface containing features of the top layer and the membrane were treated with air plasma (Harrick Plasma Inc) and brought in conformal contact to achieve irreversible bonding upon additional 30 minutes of incubation at 80 °C. The inlet for the actuation compartment was thus punched on the top layer/membrane unit (defining the cell culture compartment) with a 500 µm biopsy puncher, upon manual alignment with the bottom layer. Finally, through a further air plasma treatment, the bottom layer was permanently bonded on the membrane side of the cell culture compartment after careful manual alignment with the top layer, and allowed to cure overnight at 80 °C.

As shown in Fig. SI1, the final device featured two compartments having similar layouts (1.6 mm wide and 10 mm long) and separated by a 750 µm thick PDMS membrane.

PEG precursors production and PEG hydrogel preparation

PEG hydrogels were produced and characterized as earlier described[66]. Briefly, 1 ml FXIII (200 U/mL, Fibrogammin, CSL Behring, Switzerland) was activated with 100 µl of thrombin (20 U/mL, Sigma-Aldrich, Switzerland) for 30 min at 37 °C and resulting activated FXIII (FXIIIa) was stored in small aliquots at −80°C. Eight-arm PEG vinylsulfone (mol wt 40kDa; NOF Europe, Germany) was functionalized with peptides that contained either a FXIII glutamine acceptor substrate (*Gln*-peptides; NQEQVSPL-ERCG-NH_2; Bachem AG, Switzerland) or matrix metalloproteinase (MMP)-degradable FXIII lysine donor substrate (*Lys-MMP$_{sensitive}$*-peptides; Ac-FKGGGPQGIWGQ-ERCG-NH_2; Bachem AG, Switzerland) resulting in *8-PEG-Gln* or *8-PEG-MMP$_{sensitive}$-Lys* precursors, respectively. A stoichiometrically balanced solution *8-PEG-Gln* and *8-PEG-MMP$_{sensitive}$-Lys* was mixed for an indicated final dry mass content of hydrogel precursors in Tris buffer (50mM Tris, pH7.6; 50mM calcium chloride) leaving spare volume of 10% v/v for the addition of cell culture medium and cells. The hydrogel cross-linking was initiated by adding 10 U/ml FXIIIa and vigorous mixing. Hydrogels were formed containing final concentrations of 2% PEG precursors and $50x10^6$ cells/ml.

Finite element analysis (FEM)

A biphasic poroelastic (BPE) finite element (FE) model of the PEG based hydrogel[25] was implemented[8,26,28,67]. The BPE model describes the equivalent mechanical behavior of a continuum resulting from the multiphase interaction of an elastic solid phase and an incompressible inviscid fluid phase. This description of the hydrogel neglects the intrinsic viscoelasticity of the solid matrix and captures exclusively the viscous effects related to the interaction between the two phases. As such, when simulating confined compression it leads to underestimating the short-term reaction forces, but accurately captures the short-term deformation field[28].

The FE analysis aimed at checking i) whether undesired lateral or longitudinal stretching of the gel could be generated and ii) if strains in the hydrogel control volume were homogeneous and consistent with the desired compression level.

Computations were performed using Abaqus Standard 6.10. (Abaqus FEA, Dassault Systemes). Software adequacy in the biomechanical description of biphasic tissues was demonstrated by Wu et al.[31] and by Meng et al[68]. As previously described, two variants of the device were produced to obtain two compression levels, corresponding to -10% or -30% nominal strains, in the construct. FE analysis focused only on the latter condition, which was potentially more critical in terms of unwanted lateral and longitudinal expansions. Consistently, the height of the hanging posts was

set to 100 μm and the gel's uncompressed height was set to 143 μm (Fig. 2a, Fig SI2). Owing to the periodic structure of the device, a repetitive unit was considered, which consisted of two posts facing each other with the PEG hydrogel volume comprised in between. Owing to the symmetry of the repetitive unit, the region of interest for the FE analysis was reduced to half a post and a quarter of the hydrogel volume and kinematic boundary conditions were imposed to account for geometrical symmetries (Fig 2a, shaded area, Fig. SI3a, Fig. SI3b). The modeled portion of the post was therefore 300 μm in width (X direction) and 150 μm in length (Y direction), with a thickness of 100 μm. The hexahedron representing the gel was 150 μm wide and 165 μm long, thus including the gel region corresponding to the gap between two adjacent posts. Post's edges in contact with the gel were chamfered to reduce geometrical discontinuities, rounding corners with a 5 μm curvature radius. The post's outer end, despite being rounded in the physical device (Fig 1b), was squared off to reduce the total number of elements after assessing negligible differences in deformation values through preliminary simulations.

Both pillar and gel were meshed using 8-node linear hexahedral elements with hybrid formulation (Abaqus C3D8PH elements). A total of 5427 elements, with an average size of 10 μm, was used for the post. The mesh was refined around the corners of the surface in contact with the gels. These, having been chamfered to reduce geometrical discontinuities, needed smaller element size (1.6 μm) to be accurately rendered as geometrical features. A total of 63954 hexahedral elements were adopted for the hydrogel. The characteristic dimension of the elements varied over the hydrogel volume: is was equal to 20 μm at the side of the gel corresponding to the culture channel's mid-line and it progressively decreased down to 1.5 μm as regions closer to the hydrogel face in contact with the post were considered, so to cope with local geometrical complexity (Fig. SI2a, Fig. SI2b).

Perfect lubrication was considered in the contact between the gel and the lateral posts; interactions between the PDMS post and the gel were modeled using a surface-to-surface contact. The top surface of the post was encastred to account for its continuity with the overhanging thick PDMS layer. The top surface of the gel was impeded to move along the Z direction simulating the presence of the top layer. A zero-pore pressure was imposed on the portions of the outer face of the hydrogel which was not in contact with the post so to allow for fluid outflow (Fig SI2c, Fig.SI2d). The mechanical properties of PDMS were described as non-linear elastic and incompressible through the Mooney-Rivlin strain energy function (equation 1):

$$W = C_1(I_1 - 3) + C_2(I_2 - 3) + \frac{1}{D}(J - 1)^2 \quad (1)$$

where I_1, and I_2 are the first and second invariant of the right Cauchy-Green strain tensor **C**, J is the determinant of the deformation gradient tensor **F** and represents the ratio between the deformed and initial volume of the material, while C_1, C_2 and D are the constitutive parameters of the model. C_1 and C_2 were set equal to 254 KPa and 146 KPa respectively, as reported in the literature concerning PDMS with a base to curing agent ratio equal to 10:1[69] while D was set equal to zero as for a perfectly incompressible material.

The PEG based hydrogel's Young Modulus was assumed equal to 0.1 MPa. This value is higher as compared to data reported in the literature for similar hydrogels, but it allowed to account for the increased resistance to compression exhibited by the hydrogel due to the negatively charged glycosaminoglycans accumulating during the CoC maturation in the construct. Poisson ratio was fixed at 0.33[70], and the specific weight of the permeating fluid to 9.965x10^{-6} N/mm3[26].

In order to model the poro-elastic behavior of the hydrogel, Abaqus requires the specific material permeability defined as $K_s = \gamma_w k$ where γ_w is the permeating fluid specific weight and k is the absolute permeability. K_s was set to 0.3 mm/s. The initial void ratio $e = dV_w/dV_g$ (where dV_w is the volume of the fluid phase and dV_g is the volume of the solid phase) was estimated by the swelling ratio of the hydrogel formulation used in this study and set to 45[69]. Complete fluid saturation was assumed for the hydrogel.

To capture the time dependent non-linear behavior of the hydrogel a transient analysis was conducted using the Soil Consolidation option in Abaqus. An automatic Δt incrementation was adopted, with a minimum value of 1x10^{-6} s. The 30% compression in the Z direction (Fig. 1a) was applied by imposing a displacement of 43 µm to the hydrogel bottom with constant velocity over a 1 s timeframe.

The strain distribution was evaluated through nominal strain components acting in the X, Y and Z directions, and calculated according to Abaqus' definition at integration points of each finite element. In particular, nominal strains are defined as:

$$\varepsilon^N = \bar{\bar{V}} - \bar{\bar{I}} = \sum_{i=1}^{3} (\lambda_i - 1)\, \bar{n}_i\, \bar{n}_i^T \qquad (2)$$

where $\bar{\bar{V}} = \sqrt{\bar{\bar{F}}\bar{\bar{F}}^T}$ is the left stretch tensor (where $\bar{\bar{F}}$ is the deviatoric deformation gradient), λ_i are the principal stretches and $\bar{n}_i$ are the principal stretch directions in the current configuration.

Nominal strains were extracted from the numerical model replicating the procedure adopted in evaluating the strain experimentally. Accounting for the non-homogeneity of the mesh a matrix containing the coordinates of 9 points randomly within the hydrogel volume was generated.

Displacement and coordinates of nodes nearest to the resulting point were used in computations. Owing to the system's symmetry strains were calculated as:

$$\varepsilon_{rr} = \frac{\left((r_i - r_{sim}) + U_r\right) - \left((r_i - r_{sim})\right)}{(r_i - r_{sim})} = \frac{U_r}{(r_i - r_{sim})} \qquad (3)$$

Where the index r indicates the r-th direction considered, r_i is the r coordinate of the node i, r_{sim} is the r coordinate of the symmetry plane and U is the node i displacement in the r direction. Mean and standard deviation where computed. The process was repeated 7 times and results averaged.

Confined compression validation

Compression field in the lateral end longitudinal direction was assessed experimentally. PEG gel was prepared as previously indicated, with polystyrene beads (diameter 10 μm) laden in the gel. A colored dye was added in the chambers to better highlight the posts profile. Images of the beads were acquired during the rest phase and upon gel compression. ImageJ software was used to post-process acquired images. Seven devices were considered. For each device, nine couples of beads were considered and for each couple the mutual distance was measured along the X and Y directions, i.e., along the width and the axial direction of the culture channel, prior and after compression. Strains in lateral and longitudinal directions were calculated as:

$$\varepsilon_{ii} = \frac{L_i' - L_i}{L_i} \qquad (4)$$

Where the index i indicates the i-th direction considered, L' and L are the measured distance after and prior to compression. Mean value and standard deviation over the nine couples of beads were assessed and used to verify computational predictions.

Device actuation and mechanical characterization

The electro-pneumatical system illustrated in Fig. SI8 was assembled to apply to the CoC model the selected mechanical stimulation pattern. It comprises two Arduino microcontroller boards (Arduino Uno R3 and Arduino Nano, ATmega328P), an air pump (TM40-A12-P23012, Topsflow), two pressure sensors (MPX5500 Series, case 867C-05, Freescale semiconductor and 26PC Series, Honeywell), a miniaturized pressure regulator (ARJ1020F Series, SMC), an integrated relay (Songle), a solenoid valve (Festo Miniature Valve MH1), a custom made stripboard, a manifold, a cylindrical Poly(methyl methacrylate) (PMMA) pressure reservoir, a resistive touchscreen (PIXNOR UNO R3 2.8 TFT Touch Screen) and a cooling fan. All components were fixed to a PMMA supporting base. In detail, the air pump was connected to the pressure reservoir so to limit its duty cycle. The activation of the pump was regulated through the Arduino Nano. The

microcontroller, receiving the value provided by the MPX5500 pressure sensor, turns on or off the pump according to the pressure level in the reservoir (1600 mmHg was set as the pump stop value, 840 mmHg as the pump start value). The pump outlet is connected to a manifold linked to the pressure reservoir, to the pressure sensor and to the pressure regulator. The Honeywell pressure sensor, after signal amplification, provides the Arduino Uno with the pressure value downstream of the pressure regulator. A parallel air-line runs from the pressure regulator to the solenoid valve. The valve aperture is regulated by the Arduino Uno. The touch screen was programmed with a user interface for the regulation of the stimulation regimen. A dedicated section provided the user with the working pressure, which can be manually adjusted. Stimulation frequencies of 0.5 Hz, 1 Hz and 2 Hz could be selected by the user. Stimulation frequency and pattern could be regulated according to each experimental design.

A ramp of stopcocks was connected to the miniature valve outlet to multiply the number of addressable microfluidic devices. Up to 24 devices have been stimulated simultaneously.

Healthy human cartilage samples collection, cell isolation and expansion

Macroscopically normal human articular cartilage was obtained from the knee joints of a total of 5 patients with unknown clinical history of joint disorders (mean donor age: 66 years; range: 54-84 years, 1 female and 4 male), after informed consent by relatives and in accordance with the local ethics committee (University Hospital Basel, Switzerland). Cartilage biopsy was minced and digested enzymatically to isolate and use cells. Briefly, human articular chondrocytes (hACs) were isolated using 0.15% type II collagenase (10 ml solution/g tissue, 300 U/mg, Worthington Biochemical Corporation, Lakewood, NJ) for 22 h and resuspended in Dulbecco's modified Eagle's medium (DMEM) containing 10% fetal bovine serum, 4.5 mg/ml D-Glucose, 0.1 mM nonessential amino acids, 1 mM sodium pyruvate, 100 mM HEPES buffer, 100 U/ml penicillin, 100 µg/ml streptomycin, and 0.29 mg/ml L-glutamine (complete medium). The isolated chondrocytes were counted using trypan blue, plated in tissue culture flasks at a density of 10^4cells/cm^2 and cultured in complete medium with the supplementation of 1 ng/ml of transforming growth factor-β1 (TGF-β1) and 5 ng/ml of fibroblast growth factor-2 (FGF-2) in a humidified 37°C/5% CO_2 incubator. The growth factor combination was selected based on the previously reported ability to increase human chondrocyte proliferation and capability to redifferentiate, even upon an initial dedifferentiating culture (41). After approximately 10 days, when cells were about 80% confluent, first passage cells (P1) were rinsed with phosphate buffered saline (PBS), detached using 0.05% trypsin/0.53 mM EDTA and replated at 5×10^3cells/cm^2. After one more week, when cells were again about 80% confluent, second passage cells (P2) were detached and exploited to generate either 2D monolayer controls or the CoC model as described below.

In order to characterize the gene expression profile of native healthy cartilage, macroscopically normal human articular cartilage was obtained from the knee joints of additional 5 patients with

unknown clinical history of joint disorders (mean donor age: 55.8 years; range: 51-60 years old, 1 female and 4 male), after informed consent by relatives and in accordance with the local ethics committee (University Hospital Basel, Switzerland). Again, cartilage biopsy was minced and digested enzymatically as aforementioned. Freshly isolated, healthy hACs from the different donors were pooled and frozen to further perform RT-PCR analysis.

OA human cartilage samples collection and analysis

Macroscopically fibrillated human articular cartilage was obtained from the knee joints of a total of 10 patients with clinical history of OA (mean donor age: 74 years; range: 55-82 years, 6 female and 4 male) undergoing a total knee replacement, after informed consent by relatives and in accordance with the local ethics committee (University Hospital Basel, Switzerland). Cartilage biopsy was minced and digested enzymatically as aforementioned. Freshly isolated, hACs from the different donors were pooled and frozen to further perform RT-PCR analysis.

Healthy human CoC model generation

The healthy human CoC model was generated by embedding hACs into an enzymatically cross-linkable and degradable poly (ethylene glycol) (PEG) based hydrogel matrix into the microscale platform. Hydrogels with a final dry mass content of 2% were prepared by stoichiometrically balanced ([Lys]/[Gln] = 1) precursor solutions of 8-PEG-Gln and 8-PEG-MMPsensitive-Lys in Tris-Buffer (TBS, 50 mM, pH 7.6) containing 50 mM calcium chloride, leaving open a spare volume of 12.5% v/v for addition of cell culture medium with hACs. The precursor solution was thus mixed to a hACs cell suspension at a final concentration of 5×10^4 cells/µl and allowed to polymerize by adding 10 U/mL thrombin-activated factor XIIIa and vigorous mixing. The cell-laden PEG pre-polymer solution was manually injected into the culture channel of the microscale platform (0.45 µl/device) (Fig. SI5a, SI6a) and incubated for 15 minutes (5% CO2 and 37 °C) before filling the lateral channels with chondrogenic medium (DMEM (Sigma Aldrich) containing 2% fetal bovine serum, 4.5 mg/ml D-Glucose, 0.1 mM nonessential amino acids, 1 mM sodium pyruvate, 100 mM HEPES buffer, 100 U/ml penicillin, 100 µg/ml streptomycin, and 0.29 mg/ml L-glutamine and supplemented with 0.1 mM ascorbic acid 2-phosphate, 10 µg/mL insulin, and 10 ng/mL TGF-β3). 3D hACs-laden microconstructs were cultured under static regimen for two weeks in chondrogenic medium (Fig.SI5b). Medium was changed every second day and collected for further analysis. Upon two weeks, samples were collected for RT-qPCR, immunofluorescence, GAG and DNA quantification analyses as described below.

Mechanical compression regimens

Upon two weeks of maturation, CoC were subjected to two different levels of confined mechanical compression for the following 7 days (Fig. SI5c). Specifically, a physiological compression (PC) of

10% and a hyper-physiological 30% compression (HPC) were chosen. A pattern resembling the daily walk routine was applied. In details, a frequency of 1Hz was chosen and the following temporal windows of stimulation applied: 2h stimulation, 4h rest, 2h stimulation, 16h rest per day (Fig. SI5c). Control devices were cultured under static conditions. Cytokine-based controls were also established. Specifically, upon two weeks of maturation, CoC were subjected to two different concentrations of IL1β for the following 7 days: a low dose of IL1β (10pg/ml, IL1β low), reported to be found in the synovial fluid of OA patients[38], and a supraphysiological dose (1ng/ml, IL1β high), previously reported to be used in 2D models[5]. A 2D cytokine-based control was finally established following traditional protocols[39]. In details, human articular chondrocytes were plated at a density of 20,000 cells/cm^2 and cultured for 10 days in complete medium. High dose of IL1β (1ng/ml) was then supplemented to the medium for seven days.

A specific experiment was performed to demonstrate the necessity of confinement. Specific unconfined compression controls were introduced. In detail a hyper-physiological 30% unconfined compression (UC) was applied through a device characterized by similar micro-scale dimensions but allowing construct lateral expansion upon compression[23]. This is possible through a different post shape and architecture, designed to channel the cell-laden hydrogel upon injection but minimizing the hindrance to lateral expansion upon compression.

In all conditions, chondrogenic medium was changed every second day and collected for further analysis. Upon seven days of stimulation, samples were collected for RT-qPCR, immunofluorescence, GAG and DNA quantification analyses as described below.

Validation of CoC model as drug screening tool

Upon two weeks of maturation and one week of HPC, the effect of different drugs was tested (Fig.SI5d). Specifically, while maintaining the hyperphysiological compression regimen, medium (free from serum, Insulin and TGFβ3 supplementation) was supplemented for three additional days with different concentrations of compounds previously shown to have anti-inflammatory and anti-degrading effects preclinical and clinical studies. In details, Dexamethasone (10μM), Interleukin-1 receptor antagonist (IL1Ra, 10ng/ml and 500ng/ml), the mTORC1 inhibitor Rapamycin (10nM, 1μM) and the non-steroidal anti-inflammatory drug Celecoxib (0.1μM) were tested. In addition, the depolymerized hyaluronic acid alkylamide HYADD®4 and a low molecular weight hyaluronic acid (≈ 50kDa), provided by Fidia Farmaceutici Spa (Italy), were tested in the system at a concentration of 1mg/ml. All drugs were diluted in DMSO, also used as vehicle (1:5000). A static device was used as “healthy control”. A cytokine-based control was finally established as described above. In details, upon two weeks of maturation and one week of high dose of IL1β (1ng/ml), the effect of IL1Ra (500ng/ml) and Rapamycin (1μM) was tested, while maintaining IL1β stimulation.

Upon three days of drug treatment, samples were collected for RT-qPCR analysis as described below.

Immunofluorescence analysis

Immunofluorescence analyses were performed on CoC models directly within the microscale platform at day0, day3, day14 and day21. Samples were fixed in 4% paraformaldehyde (PFA) overnight at 4°C. Subsequently, the microscale platform was disassembled by removing the actuation compartment and carefully pealing-off the PDMS membrane from the culture compartment, eventually exposing the CoC model. Cells were permeabilized with 0.3% Tween (Sigma) PBS solution for 10 minutes. A blocking solution (3% bovine serum albumin (BSA), 0.5% Triton (Sigma) in PBS) was applied for 1 hour at room temperature to block nonspecific bindings. Samples were incubated overnight at 4°C with primary antibodies. Rabbit anti-human aggrecan (dilution 1:200, Abcam), mouse anti-human collagen type-I (dilution 1:200, Abcam) and mouse anti-human collagen type-II (dilution 1:200, Abcam) were used to evaluate the maturation of CoC at day0, day3 and day14. rabbit anti-human MMP-13 (dilution 1:200, Abcam) and mouse anti-human DIPEN (dilution 1:200, MDBioscience) were used to assess the effect of mechanical compression on CoC model. DAPI staining was used to identify the cell nuclei. As appropriate, secondary antibodies labeled with Alexa Fluo 488, Alexa Fluo 546, Alexa Fluo 647 (Invitrogen) were used at 1:200 for 45 minutes at room temperature.
Representative images of three different regions of each CoC model were acquired with a 20x objective with fluorescence Nikon A1R Nala Confocal microscope (Nikon, Tokyo, Japan), and analyzed by using ImageJ software. Three donors were considered, with three technical replicates per donor for each condition and time point.

Biochemical analyses

Samples were extracted from the microscale platform and digested in 300 mL of proteinase-K (1 mg/mL proteinase-K in 50 mM Tris with 1 mM EDTA, 1 mM iodoacetamide, and 10 µg/mL pepstatin-A) overnight at 56°C. GAG amounts were measured spectrophotometrically after reaction with dimethylmethylene blue using chondroitin sulfate as a standard [71]. The amount of DNA was measured spectrophotometrically using the CyQuant cell proliferation assay Kit (Molecular Probes, Eugene, OR), according to manufacturer's instructions. GAG contents were reported as GAG/DNA. Three donors were considered, with three technical replicates per donor each time point.

Quantitative real-time reverse transcriptase polymerase chain reaction (RT-PCR)

Total RNA extraction by Trizol, cDNA synthesis and real-time reverse transcriptase-polymerase chain reaction (RT-PCR; 7300 AB Applied Biosystem) were performed according to standard

protocol to quantitate expression levels of the following genes of interest (Applied Biosystems): *COL2A1* (Hs00264051_m1), *COL1A1 (*Hs00164004_m1), *ACAN* (Hs00153936_m1), *PRG4* (Hs00981633_m1), *GDF5* (Hs00167060_m1), *ATX* (Hs00905117_m1), *FRZB* (Hs00173503_m1), *GREM1* (Hs01879841_s1), *MMP13* (Hs00233992_m1), *IL6* (Hs00985639_m1), *IL8* (Hs00174103_m1), *COL10A1* (Hs00166657_m1), *IHH* (Hs01081800_m1), *DKK-1* (Hs00183740_m1). The house-keeping gene Glyceraldehyde 3-phosphate dehydrogenase (*GAPDH*) was used as reference (Hs02758991_g1). Five donors were considered, with three technical replicates per donor each condition and time point.

MMP-13 release quantification

MMP-13 production was selectively assayed using enzyme specific fluorescence substrate kits SensoLyte 520 MMP13 Assay Kit (AnaSpec Fremont, CA 94555), according to manufacturer's instructions. Briefly, cell supernatants were collected at days 16, 18, 20 and 21 during the mechanical compression phase and the time point pooled to measure the accumulation of MMP-13 during the whole stimulation period. The kit uses 96-well plates coated with a monoclonal anti-human MMP-13 antibody that recognizes both the latent and active forms of the enzyme. The specificity of the monoclonal antibodies prevents cross-reactivity with other MMPs. Pro-MMP-13 is activated by incubation with 4-aminophenylmercuric acetate (APMA) at 37 °C. Proteolytic activity of the enzymes is measured using a fluorescence resonance energy transfer (FRET) peptide containing a quenched fluorophore. Upon cleaving MMP-13, fluorescence of the fluorophore was recovered and was measured on configurable multi-mode microplate reader (Synergy H1, Biotek Instruments GmbH) following a five hours incubation period at room temperature, with an excitation and emission wavelength of 485±20 nm and 530±25 nm, respectively. Three donors were considered, with three technical replicates per donor for each condition.

Statistical analysis

Results of computational simulations and strain field validation are presented as median ± IQR. Results of quantitative RT-qPCR, biochemical analyses and proMMP-13 quantification are presented as mean ± SD. Statistical analysis was performed using GraphPad Prism 7.00 for Mac. Data Populations normal distribution was assessed through D'Agostino-Pearson Test. Two tailed Student's T-test (normal distributions) and Mann-Whitney test (non-normal distributions) where used when comparing two populations. Multiple comparisons were realized using ordinary one way ANOVA. When comparing normally distributed variables, Bonferroni's or Dunnett's multiple comparison tests with single pooled variance were used for small or large numbers of populations and statistical significance was indicated by $P<0.05$ (*) and $P<0.01$(**), respectively. When comparing non-normally distributed variables, the Kruskal-Wallis test with Dunn's multiple

comparison test was used and statistical significance was indicated by P<0.001(***) and P<0.0001(****), respectively.

Data availability

The authors declare that all data supporting the findings of this study are available within the paper and its Supplementary Information. The data that support the findings of this study are available from the corresponding author upon reasonable request.

References

1. Bijlsma, J. W., Berenbaum, F. & Lafeber, F. P. Osteoarthritis: an update with relevance for clinical practice. *Lancet* **377,** 2115–2126 (2011).

2. Wittenauer, R., Smith, L. & Aden, K. Background Paper 6.12 Osteoarthritis. (2013).

3. Sanchez-Adams, J., Leddy, H. A., McNulty, A. L., O'Conor, C. J. & Guilak, F. The Mechanobiology of Articular Cartilage: Bearing the Burden of Osteoarthritis. *Curr. Rheumatol. Rep.* **16,** 451 (2014).

4. Arden, N. & Nevitt, M. C. Osteoarthritis: Epidemiology. *Best Pract. Res. Clin. Rheumatol.* **20,** 3–25 (2006).

5. Johnson, C. I., Argyle, D. J. & Clements, D. N. In vitro models for the study of osteoarthritis. *Vet. J.* **209,** 40–49 (2016).

6. Esch, E. W., Bahinski, A. & Huh, D. Organs-on-chips at the frontiers of drug discovery. *Nat. Rev. Drug Discov.* **14,** 248–260 (2015).

7. Kutzner, I. *et al.* Loading of the knee joint during activities of daily living measured in vivo in five subjects. *J. Biomech.* **43,** 2164–2173 (2010).

8. Mow, V. C., Ratcliffe, A. & Robin Poole, A. Cartilage and diarthrodial joints as paradigms for hierarchical materials and structures. *Biomaterials* **13,** 67–97 (1992).

9. Grodzinsky, A. J., Levenston, M. E., Jin, M. & Frank, E. H. Cartilage tissue remodelling in response to mechanical forces. **Annu. Rev.,** 691–713 (2000).

10. Choi, J. B. *et al.* Zonal changes in the three-dimensional morphology of the chondron under compression: The relationship among cellular, pericellular, and extracellular deformation in articular cartilage. *J. Biomech.* **40,** 2596–2603 (2007).

11. Lin, H., Lozito, T. P., Alexander, P. G., Gottardi, R. & Tuan, R. S. Stem cell-based microphysiological osteochondral system to model tissue response to interleukin-1?? *Mol. Pharm.* **11,** 2203–2212 (2014).

12. Goldman, S. M. & Barabino, G. A. Spatial Engineering of Osteochondral Tissue Constructs Through Microfluidically Directed Differentiation of Mesenchymal Stem Cells. *Biores. Open Access* **5,** 109–117 (2016).

13. Mumme, M. *et al.* Nasal chondrocyte-based engineered autologous cartilage tissue for repair of articular cartilage defects: an observational first-in-human trial. *Lancet* **388,** 1985–1994 (2016).

14. Kafienah, W. *et al.* Three-Dimensional Tissue Engineering of Hyaline Cartilage: Comparison of Adult Nasal and Articular Chondrocytes. *Tissue Eng.* **8,** 817–826 (2002).

15. Tsimbouri, P. M. *et al.* Stimulation of 3D osteogenesis by mesenchymal stem cells using a nanovibrational bioreactor. *Nat. Biomed. Eng.* **1,** 758–770 (2017).

16. Lee, D. A. & Bader, D. L. Compressive strains at physiological frequencies influence the metabolism of chondrocytes seeded in agarose. *J. Orthop. Res.* **15,** 181–188 (1997).

17. De Croos, J. N. A., Dhaliwal, S. S., Grynpas, M. D., Pilliar, R. M. & Kandel, R. A. Cyclic compressive mechanical stimulation induces sequential catabolic and anabolic gene changes in chondrocytes resulting in increased extracellular matrix accumulation. *Matrix Biol.* **25,** 323–331 (2006).

18. Khozoee, B., Mafi, P., Mafi, R. & Khan, W. Mechanical Stimulation Protocols of Human Derived Cells in Articular Cartilage Tissue Engineering – A Systematic Review. *Curr. Stem*

Cell Res. Ther. **12,** 260–270 (2017).

19. Huh, D. *et al.* Reconstituting organ-level lung functions on a chip. *Science (80-.).* **328,** 1662–1668 (2010).

20. Ugolini, G. S., Visone, R., Redaelli, A., Moretti, M. & Rasponi, M. Generating Multicompartmental 3D Biological Constructs Interfaced through Sequential Injections in Microfluidic Devices. *Adv. Healthc. Mater.* **6,** (2017).

21. Occhetta, P., Visone, R. & Rasponi, M. High-throughput microfluidic platform for 3D cultures of mesenchymal stem cells. *Methods Mol. Biol.* **1612,** 303–323 (2017).

22. Ng, J. M. K., Gitlin, I., Stroock, A. D. & Whitesides, G. M. Components for integrated poly(dimethylsiloxane) microfluidic systems. *Electrophoresis* **23,** 3461–3473 (2002).

23. Marsano, A. *et al.* Beating heart on a chip: a novel microfluidic platform to generate functional 3D cardiac microtissues. *Lab Chip* **16,** 599–610 (2016).

24. Visone, R. *et al.* A Simple Vacuum-Based Microfluidic Technique to Establish High-Throughput Organs-On-Chip and 3D Cell Cultures at the Microscale. *Adv. Mater. Technol.* 1800319 (2018). doi:10.1002/admt.201800319

25. Ehrbar, M. *et al.* Biomolecular hydrogels formed and degraded via site-specific enzymatic reactions. *Biomacromolecules* **8,** 3000–3007 (2007).

26. Blum, M. M. & Ovaert, T. C. Experimental and numerical tribological studies of a boundary lubricant functionalized poro-viscoelastic PVA hydrogel in normal contact and sliding. *J. Mech. Behav. Biomed. Mater.* **14,** 248–258 (2012).

27. Kalyanam, S. Poro-Viscoelastic Behavior of Gelatin Hydrogels Under Compression-Implications for Bioelasticity Imaging. *J. Biomech. Eng.* **131,** 81005 (2009).

28. DiSilvestro, M. R., Zhu, Q., Wong, M., Jurvelin, J. S. & Suh, J.-K. F. Biphasic Poroviscoelastic Simulation of the Unconfined Compression of Articular Cartilage: I—Simultaneous Prediction of Reaction Force and Lateral Displacement. *J. Biomech. Eng.* **123,** 191 (2001).

29. Villanueva, I., Hauschulz, D. S., Mejic, D. & Bryant, S. J. Static and dynamic compressive strains influence nitric oxide production and chondrocyte bioactivity when encapsulated in PEG hydrogels of different crosslinking densities. *Osteoarthr. Cartil.* **16,** 909–918 (2008).

30. Phelps, E. A. *et al.* Maleimide cross-linked bioactive PEG hydrogel exhibits improved reaction kinetics and cross-linking for cell encapsulation and in situ delivery. *Adv. Mater.* **24,** 64–70 (2012).

31. Wu, J. Z., Herzog, W. & Epstein, M. Evaluation of the finite element software ABAQUS for biomechanical modelling of biphasic tissues. *J. Biomech.* **31,** 165–169 (1997).

32. Ray, A., Singh, P. N. P., Sohaskey, M. L., Harland, R. M. & Bandyopadhyay, A. Precise spatial restriction of BMP signaling is essential for articular cartilage differentiation. *Development* **142,** 1169–1179 (2015).

33. Nishioka, T. *et al.* ATX-LPA1 axis contributes to proliferation of chondrocytes by regulating fibronectin assembly leading to proper cartilage formation. *Sci. Rep.* **6,** 23433 (2016).

34. Leijten, J. C. H. *et al.* Gremlin 1, Frizzled-related protein, and Dkk-1 are key regulators of human articular cartilage homeostasis. *Arthritis Rheumatol.* **64,** 3302–3312 (2012).

35. Takaishi, H., Kimura, T., Dalal, S., Okada, Y. & D'Armiento, J. Joint diseases and matrix metalloproteinases: a role for MMP-13. *Curr. Pharm. Biotechnol.* **9,** 47–54 (2008).

36. Flory, J. J. E., Fosang, A. J. & Knudson, W. The Accumulation of Intracellular ITEGE and

DIPEN Neoepitopes in Bovine Articular Chondrocytes Is Mediated by CD44 Internalization of Hyaluronan. *Arthritis Rheum.* **54,** 443–454 (2006).

37. Kronenberg, H. M. Developmental regulation of the growth plate. *Nature* **423,** 332–336 (2003).

38. Tsuchida, A. I. *et al.* Cytokine profiles in the joint depend on pathology, but are different between synovial fluid, cartilage tissue and cultured chondrocytes. *Arthritis Res. Ther.* **16,** 441 (2014).

39. Bau, B. *et al.* Relative messenger RNA expression profiling of collagenases and aggrecanases in human articular chondrocytes in vivo and in vitro. *Arthritis Rheumatol.* **46,** 2648–2657 (2002).

40. Leijten, J. C. H. *et al.* GREM1, FRZB and DKK1 mRNA levels correlate with osteoarthritis and are regulated by osteoarthritis-associated factors. *Arthritis Res. Ther.* **15,** R126 (2013).

41. Braddock, M. & Quinn, A. Targeting IL-1 in inflammatory disease: new opportunities for therapeutic intervention. *Nat. Rev. Drug Discov.* **3,** 330 (2004).

42. Grodzinsky, A. J., Wang, Y., Kakar, S., Vrahas, M. S. & Evans, C. H. Intra-articular dexamethasone to inhibit the development of post-traumatic osteoarthritis. *J. Orthop. Res.* **35,** 406–411 (2017).

43. Lim, H. *et al.* Inhibition of matrix metalloproteinase-13 expression in IL-1β-treated articular chondrocytes by a steroidal saponin, spicatoside A, and its cellular mechanisms of action. *Arch. Pharm. Res.* **38,** 1108–1116 (2015).

44. Yan, B. *et al.* mTORC1 regulates PTHrP to coordinate chondrocyte growth, proliferation and differentiation. *Nat. Commun.* **7,** 11151 (2016).

45. Pal, B., Endisha, H., Zhang, Y. & Kapoor, M. mTOR: a potential therapeutic target in osteoarthritis? *Drugs R. D.* **15,** 27–36 (2015).

46. Sasaki, H. *et al.* Autophagy modulates osteoarthritis-related gene expression in human chondrocytes. *Arthritis Rheumatol.* **64,** 1920–1928 (2012).

47. Zweers, M. C. *et al.* Celecoxib: considerations regarding its potential disease-modifying properties in osteoarthritis. *Arthritis Res. Ther.* **13,** 239 (2011).

48. Pavan, M., Galesso, D., Secchieri, C. & Guarise, C. Hyaluronic acid alkyl derivative: a novel inhibitor of metalloproteases and hyaluronidases. *Int. J. Biol. Macromol.* **84,** 221–226 (2016).

49. Pavan, M., Galesso, D., Menon, G., Renier, D. & Guarise, C. Hyaluronan derivatives: Alkyl chain length boosts viscoelastic behavior to depolymerization. *Carbohydr. Polym.* **97,** 321–326 (2013).

50. Kapoor, M., Martel-Pelletier, J., Lajeunesse, D., Pelletier, J.-P. & Fahmi, H. Role of proinflammatory cytokines in the pathophysiology of osteoarthritis. *Nat. Rev. Rheumatol.* **7,** 33 (2011).

51. Guarise, C. *et al.* Matrix metalloprotease 3 (MMP3) inhibition effect of a viscosupplement based on a hyaluronic acid amide derivative (HYADD4). *Osteoarthr. Cartil.* **26,** S286–S287 (2018).

52. Moraes, C., Sun, Y. & Simmons, C. A. (Micro) managing the mechanical microenvironment. *Integr. Biol.* **3,** 959–971 (2011).

53. Greaves, L. L., Gilbart, M. K., Yung, A. C., Kozlowski, P. & Wilson, D. R. Effect of acetabular labral tears, repair and resection on hip cartilage strain: A 7 T MR study. *J. Biomech.* **43,**

858–863 (2010).

54. Wong, B. L. & Sah, R. L. Effect of a focal articular defect on cartilage deformation during patello-femoral articulation. *J. Orthop. Res.* **28,** 1554–1561 (2010).

55. Lutolf, M. P. & Hubbell, J. a. Synthetic biomaterials as instructive extracellular microenvironments for morphogenesis in tissue engineering. *Nat. Biotechnol.* **23,** 47–55 (2005).

56. Barbero, A. *et al.* Age related changes in human articular chondrocyte yield, proliferation and post-expansion chondrogenic capacity. *Osteoarthr. Cartil.* **12,** 476–484 (2004).

57. Nam, J., Aguda, B. D., Rath, B. & Agarwal, S. Biomechanical Thresholds Regulate Inflammation through the NF-κB Pathway: Experiments and Modeling. *PLoS One* **4,** e5262 (2009).

58. Hunter, C. J., Imler, S. M., Malaviya, P., Nerem, R. M. & Levenston, M. E. Mechanical compression alters gene expression and extracellular matrix synthesis by chondrocytes cultured in collagen I gels. *Biomaterials* **23,** 1249–1259 (2002).

59. Dreier, R. Hypertrophic differentiation of chondrocytes in osteoarthritis: the developmental aspect of degenerative joint disorders. *Arthritis Res. Ther.* **12,** 216 (2010).

60. Zhong, L. *et al.* Nitric oxide mediates crosstalk between interleukin 1β and WNT signaling in primary human chondrocytes by reducing DKK1 and FRZB expression. *Int. J. Mol. Sci.* **18,** 1–18 (2017).

61. Mobasheri, A., Bay-Jensen, A.-C., van Spil, W. E., Larkin, J. & Levesque, M. C. Osteoarthritis Year in Review 2016: biomarkers (biochemical markers). *Osteoarthr. Cartil.* **25,** 199–208 (2017).

62. Goldring, S. R. & Goldring, M. B. Changes in the osteochondral unit during osteoarthritis: structure, function and cartilage–bone crosstalk. *Nat. Rev. Rheumatol.* **12,** 632–644 (2016).

63. Yuan, X. L. *et al.* Bone-cartilage interface crosstalk in osteoarthritis: potential pathways and future therapeutic strategies. *Osteoarthr. Cartil.* **22,** 1077–89 (2014).

64. Takayama, K. *et al.* Local intra-articular injection of rapamycin delays articular cartilage degeneration in a murine model of osteoarthritis. *Arthritis Res. Ther.* **16,** 482 (2014).

65. Matsuzaki, T. *et al.* Intra-articular administration of gelatin hydrogels incorporating rapamycin–micelles reduces the development of experimental osteoarthritis in a murine model. *Biomaterials* **35,** 9904–9911 (2014).

66. Lienemann, P. S., Lutolf, M. P. & Ehrbar, M. Biomimetic hydrogels for controlled biomolecule delivery to augment bone regeneration. *Adv. Drug Deliv. Rev.* **64,** 1078–1089 (2012).

67. DiSilvestro, M. R. & Suh, J. K. F. A cross-validation of the biphasic poroviscoelastic model of articular cartilage in unconfined compression, indentation, and confined compression. *J. Biomech.* **34,** 519–525 (2001).

68. Meng, Q., Jin, Z., Fisher, J. & Wilcox, R. Comparison between FEBio and Abaqus for biphasic contact problems. *Proc. Inst. Mech. Eng. Part H J. Eng. Med.* **227,** 1009–1019 (2013).

69. Ehrbar, M. *et al.* Elucidating the Role of Matrix Stiffness in 3D Cell Migration and Remodeling. *Biophys. J.* **100,** 284–293 (2011).

70. Phelps, E. A. *et al.* Maleimide cross-linked bioactive PEG hydrogel exhibits improved reaction kinetics and cross-linking for cell encapsulation and in-situ delivery.

doi:10.1002/adma.201103574

71. Farndale, R. W., Buttle, D. J. & Barrett, A. J. Improved quantitation and discrimination of sulphated glycosaminoglycans by use of dimethylmethylene blue. *Biochim. Biophys. Acta (BBA)-General Subj.* **883,** 173–177 (1986).

Acknowledgements

We are grateful to Dr. G. Pagenstert for the kind provision of articular cartilage biopsies. We are grateful to Fidia Farmaceutici Spa (Italy) for the kind provision of HYADD®4 and LMW-HA compounds, and in particular to Dr. Devis Galesso, Dr. Riccardo Beninatto and Dr. Cristian Guarise for their precious feedbacks on the results. This work was partially funded by the Swiss National Science Foundation (SNSF numbers 310030-126965.1 and 310030_149614/1).

Author contribution

M.R., A.B. and P.O. conceived the project; M.R. and A.M. conceived the device; E.V. and A.M. implemented the FEM model and performed simulations; A.M. performed the mechanical characterization of the device; A.M and P.O. produced the devices; P.O. and A.M. performed and analysed the biological experiments; Q.V.M. and M.E. produced the PEG gel; P.O., A.M., M.R., A.B. and I.M. wrote the manuscript; the authors discussed the results, commented on the manuscript and contributed to its final version.